Colloidal gold nanosphere dispersions in smectic liquid crystals and thin nanoparticle-decorated smectic films

R. Pratibha,[1,2,3] W. Park,[2] and I. I. Smalyukh[1,4,5,a)]
[1]*Department of Physics, University of Colorado, Boulder, Colorado 80309, USA*
[2]*Department of Electrical and Computer Engineering, University of Colorado, Boulder, Colorado 80309, USA*
[3]*Raman Research Institute, C.V. Raman Avenue, Bangalore 560080, India*
[4]*Liquid Crystal Materials Research Center, University of Colorado, Boulder, Colorado 80309, USA*
[5]*Renewable and Sustainable Energy Institute, University of Colorado, Boulder, Colorado 80309, USA*

(Received 11 November 2009; accepted 27 January 2010; published online 24 March 2010)

We demonstrate that the layer structure and elasticity stabilize dispersions of colloidal nanoparticles in smectic liquid crystals. We use surface plasmon resonance spectra of gold nanospheres to probe their spatial distributions in the bulk of smectic lamellae. The average interparticle distances between the well-separated nanoinclusions in thin (<100 nm) smectic films are probed by atomic force microscopy. We show that limited motion of nanoparticles across layers due to the one-dimensional quasi-long-range solid-like structure and their elasticity-mediated interactions preclude irreversible aggregation and enhance the stability of the ensuing nanoscale dispersions in thermotropic smectic liquid crystals. © *2010 American Institute of Physics*.
[doi:10.1063/1.3330678]

I. INTRODUCTION

Dispersions of colloidal particles in anisotropic liquid crystalline media are interesting from both fundamental physics and technological applications standpoints. Studies of colloidal microparticles in nematic[1–5] and smectic[6–11] liquid crystals (LCs) reveal strongly anisotropic long-range interactions that can be of both attractive and repulsive nature.[2] The interactions depend on topological defects and *director* structures occurring around the particles and are mediated by orientational elasticity of the surrounding LC medium. In the case of micron-sized inclusions embedded in a nematic LC, both dipolar and quadrapolar configurations can occur, depending on the surface anchoring of the *director*.[1] When the orientation of the "easy axis" of the *director* is normal to the surface of the inclusion, linear colloidal chains are formed owing to the long-range dipolar attractive interaction. The short range repulsive interaction associated with the hyperbolic point defects close to the colloidal particles prevents aggregation or coalescence. When the surface anchoring at the LC-colloid interface is weak vertical or planar, more complex structures form due to *director* distortions of a quadrapolar symmetry, such as the ones involving saturn ring line defects[5] or surface point defects called boojums.[4] These interactions often result in aggregation of particles into chains at a certain angle with respect to the far-field director. When the particle size is <100 nm and smaller than (or comparable to) the surface anchoring extrapolation length, all spherical particles induce director distortions of quadrupolar symmetry and thus elasticity-mediated forces in anisotropic fluids like nematics facilitate their anisotropic aggregation.

Colloidal inclusions in smectics distort the surrounding ground-state structure of uniform LC *director* and equidistant lamellae.[6–11] These elastic distortions of the layered structure can also result in elasticity-mediated interparticle interactions. However, it is not known if stable dispersions of nanoparticles in such systems are possible. In this work, we use colloidal metal nanospheres[12] to show that the nanoparticle dispersions in smectics can be stabilized against aggregation both in the bulk and in thin smectic films. Stability of colloidal dispersions and average interparticle distances in thick bulk samples are probed by analyzing surface plasmon resonance (SPR) spectra. Isolated non-aggregating colloids in thin smectic films formed by LC-nanosphere dispersions are revealed by atomic force microscopy (AFM) studies of their surface topography. We demonstrate that the nanoscale dispersions of well-separated colloids in the smectic A anisotropic matrix are stabilized by the limited motion of nanospheres across the layers due to the one-dimensional (1D) quasi-long-range translational order and elastic interparticle interactions.

II. EXPERIMENTAL METHODS AND MATERIALS

The smectogenic LC 4-*n*-octyl 4′-cyanobiphenyl (8CB, from Frinton Laboratories, Inc., Moorestown, NJ) used in our studies exhibits the following phase sequence: crystal phase (21 °C)–SmA LC phase (32 °C)–nematic phase (40.5 °C)–isotropic phase. Gold nanoparticles (GNPs) of radius 7 nm (as measured using scanning electron microscope images) were initially obtained in an aqueous medium using a standard synthetic procedure.[12,13] The nanoparticles were then coated with the amphiphilic, nonionic polymer poly (N-vinyl-2-pyrrolidone) (PVP 10 from Aldrich) and transferred to ethyl alcohol to reduce the chances of aggregation and facilitate better dispersion of the particles in the LC medium. In order to obtain dispersions with various volume fractions

a)Electronic mail: ivan.smalyukh@colorado.edu.

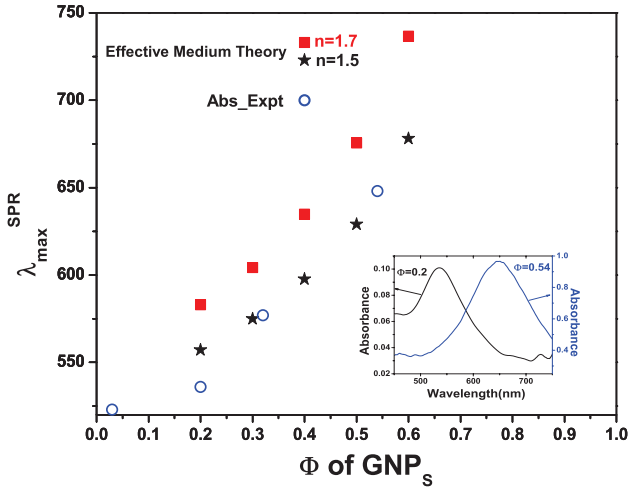

FIG. 1. (Color online) Dependence of SPR wavelength λ^{SPR}_{max} on volume fraction Φ of GNPs. Solid symbols correspond to λ^{SPR}_{max} obtained from simulations taking different values of refractive index. Open circles correspond to λ^{SPR}_{max} obtained experimentally from absorption measurements. Inset shows typical experimental absorption spectra used to obtain λ^{SPR}_{max}.

(Φ) of GNPs, the suspension of the PVP coated GNPs in ethyl alcohol was mixed with the LC in the smectic A phase and the mixture was continuously stirred for about 5 h. For the optical absorption studies most of the ethyl alcohol was evaporated and the mixture filled into cells made of rubbed glass plates with thin polyimide alignment coatings. The remaining alcohol was allowed to evaporate over a few hours. Well-aligned smectic A samples with the *director* along the rubbing direction were obtained. The absorption spectra in the smectic A phase (at 24 °C) were obtained using the Ocean Optics miniature fiber optic spectrometer (USB2000) integrated with a polarizing microscope Olympus BX51 (Tokyo, Japan). For the AFM studies, the mixture of the PVP coated GNPs in ethyl alcohol and LC which was homogenized by continuous stirring for 5 h was spin coated at 3000 revolutions per minute on a silicon (Si) substrate. The sample surface morphology was studied using nanoscope III AFM (from Digital Instruments) in the tapping mode. To measure the average film thickness of the smectic surface-supported layers, we have used a Multiskop ellipsometer from Optrel (Sinzing, Germany).

III. RESULTS AND DISCUSSION

The LC-GNP dispersions were first characterized by optical microscopy revealing no aggregation and then further probed by measuring optical extinction spectra for the planar-aligned GNP-doped smectic A samples. The SPR peak wavelength λ^{SPR}_{max} of dispersed metal nanoparticles[14,15] was obtained from the spectra for dispersions having various volume fractions of GNPs (Fig. 1). The inset of Fig. 1 shows typical absorption spectra used to obtain the value of λ^{SPR}_{max}, which progressively shifts to longer wavelengths with increase in the volume fraction of GNPs. The experimental values of λ^{SPR}_{max} were then compared with those obtained from the Maxwell Garnet effective medium theory. The polarizability of individual GNPs was first obtained using the Mie theory[15] and the complex effective index for the composite structure was then calculated by applying the Maxwell–Garnett mixing rule.[16] The absorption spectra were obtained directly from the imaginary part of the effective index. The calculated λ^{SPR}_{max} increases with increasing volume fraction of the GNPs, similar to the experimental λ^{SPR}_{max} (Fig. 1). The calculations have been performed assuming refractive indices $n=1.7$ and $n=1.5$ corresponding to the extraordinary and ordinary refractive indices of the used LC, respectively. In the LC-GNP dispersions, the nanoparticles induce elastic *director* distortions caused by the surface anchoring at particle-LC interfaces. Hence the *director* orientation in the close vicinity of the particles departs from that imposed by rubbing of the bounding glass plates. Therefore, in principle, the calculations should consider an effective refractive index accounting for these distortions. The matching of the experimental values with the calculations considering $n=1.5$ indicates that the effective refractive LC index around GNPs is closer to the ordinary refractive index (Fig. 1). This agreement between the experimental and calculated concentration dependences of λ^{SPR}_{max} also implies that the GNPs are well-dispersed in the smectic A matrix.

In order to get further insights into the structure of these nanoscale colloidal dispersions, the LC-nanoparticle composites were prepared in the form of surface-supported thin films and the surface morphology of the film-air interface was examined by AFM. For comparison purposes, we first conducted these studies for pure 8CB samples without GNPs. The smectic A film was obtained on a Si wafer by spin coating a dilute 0.1 mM solution of 8CB in dichloromethane. The average film thickness of ~50 nm was measured using an ellipsometer and assuming that the film refractive index is equal to the ordinary refractive index of 8CB. Characteristic defect-induced depressions occurring as a result of antagonistic boundary conditions [Fig. 2(a)] at the air/LC (vertical) and substrate/LC (planar) have been observed [Fig. 2(b)], in agreement with previous studies.[17,18] Similar thin films deposited on Si substrates were prepared by spin coating the suspensions of PVP-capped GNPs in a homogenized mixture of ethyl alcohol and 8CB. The obtained films had orientation of smectic layers predominantly parallel to the substrate. Figure 3(a) shows a schematic representation of a thin smectic film incorporating nanoparticles and the morphology of top smectic layers probed by an AFM tip. In contrast to the surface depressions obtained with pure 8CB samples [Fig. 2(b)], raised bumplike regions are observed for the films of LC-GNP dispersions [Figs. 3(b)–3(d)]. The distance between the peaks decreases with increasing volume fraction. Lateral dimensions of the bumps due to particles embedded into the layered structure appear larger than the particle size because of the continuous elastic deformation of the layers above the nanoparticle and also due to the smearing effect caused by the AFM tip. Since the size of inclusions (average diameter ≈14 nm) is larger than the layer spacing of ≈3 nm, the layers in the vicinity of inclusions are displaced upwards along the layer normal (Fig. 3). The surface morphology exhibited by pure 8CB films [Figs. 3(e) and 3(f)] and the nanoparticle-decorated films is very different [Figs. 3(g) and 3(h)], although the films have been spin coated in the same way. The sections of

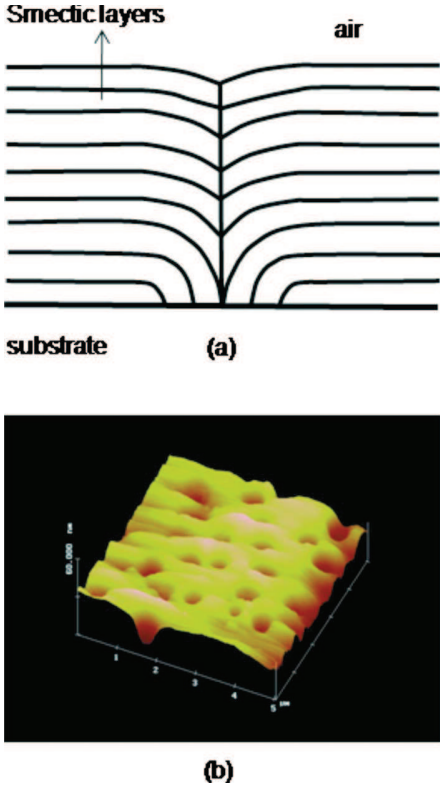

FIG. 2. (Color online) (a) Schematic representation of a toroidal focal conic domain giving rise to defect-induced dimples in the smectic film surface morphology and (b) the surface profile with the dimples obtained by AFM imaging of the 8CB thin film.

the surface profile show the defect-induced dimples in the case of pure 8CB [Fig. 3(f)] and the raised bumps due to particle-induced layer deformations in the case of the LC-GNP dispersions [Fig. 3(h)]. Since the smectic A material is a 1D solid that possesses a quasi-long-range translational order in the direction perpendicular to layers, the surface morphology visualized by AFM reflects the profile of the top smectic layer in the thin film. The apparent variation in the height of individual bumps might be due to polydispersity of particle sizes (transmission electron microscopy data show that particle diameters vary from 12 to 22 nm with an average size of ~14 nm), formation of dislocation loops of different Burgers vector encircling the nanoparticles, or location of these inclusions at different depths across the film. The interbump distance in the surface profiles decreases with increasing nanoparticle concentration [Figs. 3(b)–3(d)] and the number density of bumps matches the values expected for isolated nanoparticles at respective doping concentrations. We, therefore, conclude that the bumps correspond to individual nanoparticles incorporated into the film. AFM images of thin films show no evidence of aggregation as the distance between nanoparticles decreases with increasing their volume fraction. The bump widths progressively shrink with an increase in the nanoparticle concentration, which is expected, considering the symmetry of layer distortions around multiple isolated particles in the LC lamellae.

The AFM images show that the incorporated nanoparticles perturb the system of flat smectic layers at distances much larger than the particle size (Fig. 3). The exact smectic

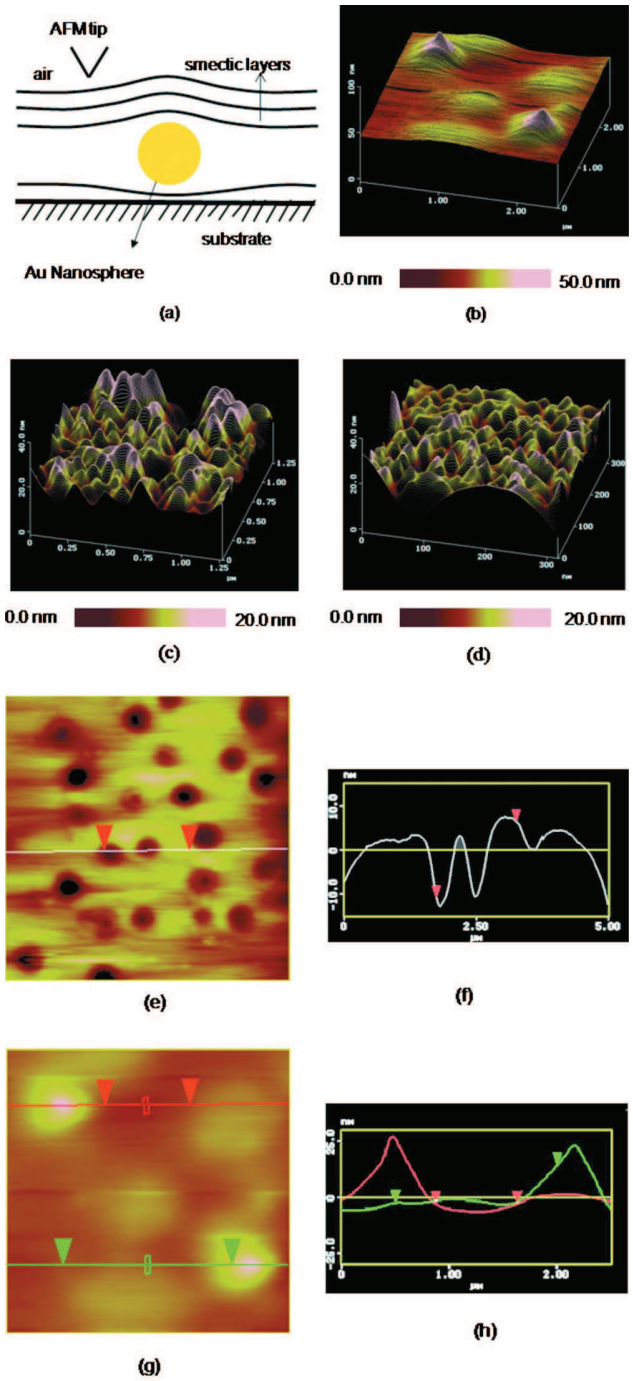

FIG. 3. (Color online) (a) Schematic representation of smectic layers with an embedded nanoparticle as probed by the AFM tip. [(b)–(d)] AFM images of the bumplike regions corresponding to layer deformation induced by nanoparticles for samples with different volume fractions Φ of GNPs and average distance (l) between the peaks: (b) $\Phi=0.03$, $L\approx2202$ nm, (c) $\Phi=0.32$, $L\approx147$ nm, and (d) $\Phi=0.54$, $L\approx36$ nm. (e) Topographical image and corresponding cross section of the depressions in the 8CB sample. (f) Topographical image and corresponding cross section of the bumps in the sample with $\Phi=0.03$ of GNPs. Note that only top and bottom layers of the smectic film are shown in (a) and that the inclusion may induce a dislocation loop encircling the nanosphere with layers terminating at the particle surface.

layer profiles around the nanoparticles are hard to visualize as the layer displacements occur on the scale of nanometers and usually model systems (such as the short-pitch cholesteric lamellae[19,20]) need to be used for this purpose. How-

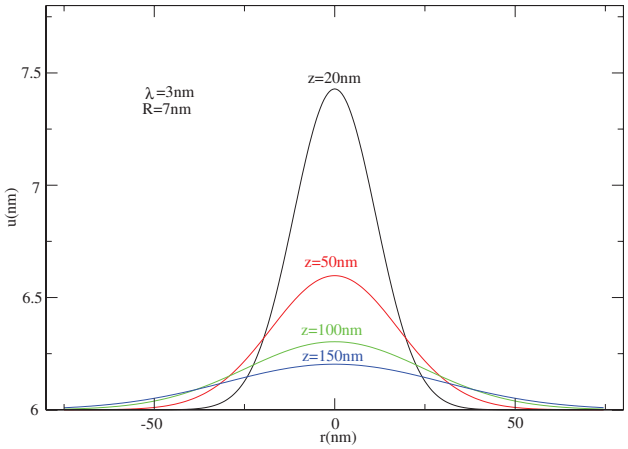

FIG. 4. (Color online) The theoretical prediction for the layer displacement as a function of the lateral distance from the particle center $\boldsymbol{r}$ for a spherical inclusion of radius $R=7$ nm. The displacement decreases on moving further away from the particle.

ever, our AFM images provide insights into the basic features of the nanoparticle-perturbed layered structures (Fig. 3). Small smectic layer deformations are usually described by the spatial variation of the layer displacement $U(\boldsymbol{r},z)$ from the ground-state flat system of lamellae. The layer displacement profiles $U(\boldsymbol{r},z)$ predicted by the nonlinear elastic theory of smectics[9] and plotted in Fig. 4 for layers 20–100 nm away from the spherical particle along the surface normal z qualitatively agree with the surface morphology of thin nanoparticle-doped smectic films (Fig. 3). This implies that the raised bumps in the AFM scans correspond to deformations induced by individual GNPs. The observed rather broad distribution of heights of these bumps may be explained by the nanoparticle locations at different depths across the smectic films as well as possible formation of the dislocation loops encircling the colloidal inclusions.

Depending on the surface confinement as well as the symmetry of layer distortions around inclusions, both attractive and repulsive elasticity-mediated interactions between the embedded particles are possible. Nanoparticles of size comparable to and larger than the smectic layer spacing induce dislocation loops and layer distortions [Fig. 5(a)] qualitatively resembling those due to the dislocation loops,[6] as shown in Fig. 5(b). When the centers of inclusions are located within the same smectic layer, their elasticity-mediated

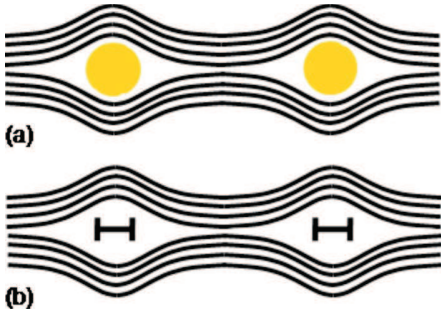

FIG. 5. (Color online) Schematic illustration of layer distortions induced by (a) two nanoparticles with possible dislocation loops around them and (b) two dislocation loops centered in the same smectic layer.

interactions are repulsive [Fig. 5(a)]. Similar to the case of dislocation loops [Fig. 5(b)], placing the nanoparticles closer to each other within the same layer implies producing stronger elastic layer curvature distortions on a shorter length scale and increasing elastic energy. The ensuing interparticle repulsion due to the elastic distortions and dislocation loops precludes their aggregation. Particle motion across the layers is hindered due to the layered structure and limited permeability. Hence, because of the elastic interactions and the layered structure, the nanoparticles do not agglomerate. This explains the enhanced stability of nanoparticle dispersions in smectic LCs as compared to the case of nematics in which the quadrupolar elasticity-mediated interactions result in irreversible anisotropic aggregation of the same GNPs. The SmA dispersions of GNPs remained stable upon sample shearing and inducing flow of the composite as well as varying temperature within the existence range of SmA phase of 8CB (21–32 °C). The stability of the dispersion of PVP-capped colloidal spheres is enhanced by smectic layered structure. For typical values of Hamaker constant for colloidal gold 2.5×10^{-19} J (Ref. 22) and 14 nm diameters of spheres, the attractive dispersion forces drop to a value comparable to K_BT when the distance between colloids is equal to that of 2–3 smectic layers.[21,22] For particle penetration across a smectic layer, a dislocation loop of radius matching that of the gold nanosphere needs to be induced in this layer. This sets a kinetic barrier $\gg K_BT$,[6] resulting in the observed smectic layer-enhanced kinetic stabilization within the temperature range of smectic LC phase.

The surface morphology of nanoparticle-doped smectic films with hybrid boundary conditions (Fig. 3) shows that the presence of nanoparticles in these films helps to avoid large-curvature defects (such as focal conic domains) and corresponding surface dimples. The nanoparticles seem to localize near to the solid surface and thus partially mitigate the effect of antagonistic surface anchoring (i.e., vertical at the LC-air interface but planar at the Si substrate). Since the particles distribute so that the in-plane interparticle distances are comparable, our findings may allow for a robust two-dimensional positioning and controlled periodic structuring of nanoparticles in the smectic thin film samples. Homogeneous dispersions with controlled structures of nanoparticles at high concentration are of special interest because of the recent emergence of the metamaterial concept.[12] Composite materials can exhibit novel optical properties at high GNP concentrations, however, such concentrated dispersions are difficult to obtain due to the agglomeration.[21] Our study shows that the GNP-smectic LC composite has a potential for self-assembly of switchable optical metamaterials. From this viewpoint, it is of special interest to further extend the scope of our studies to ferroelectric smectic LCs and to particles of nonspherical custom-designed shapes.[23] Furthermore, the nanosized inclusions immersed in smectics are expected to interact with edge dislocation and their loops,[6] which may provide additional means for nanoscale spatial localization of nanoparticles in smectics. On the other hand, since the highest achieved volume fraction of ~0.5 of PVP-capped GNPs in smectics approaches the volume fraction range at which one expects ordered structural organization even for solid

sphere dispersions in isotropic fluids, it is of great fundamental interest to explore the feasibility of achieving ordered periodic self-assembly of nanoparticles[24] and spatial structures composed of nanoparticles and particle-like structures[25,26] in lamellar LCs.

IV. CONCLUSIONS

In conclusion, we have demonstrated the enhanced colloidal stability of smectic A LC nanoparticle dispersions as compared to those in nematics. Using experimental and computer-simulated SPR spectra, we have shown that the interparticle separations between isolated metal nanoparticles in the bulk of smectic lamellae remain large even for highly concentrated suspensions. Nanoparticles in thin films also do not agglomerate but rather modify the free surface profile of the film due to layer distortions around the inclusions in the LC bulk. The nanoscale dispersions are of interest for technologies that require composites consisting of nanoparticles and a dielectric matrix with tunable properties and interparticle distances, which may provide means of spatial structuring of smectic-nanoparticle composites.

ACKNOWLEDGMENTS

We acknowledge the support of the International Institute for Complex Adaptive Matter (ICAM-I2CAM), University of Colorado Innovation seed grant, Renewable and Sustainable Energy Institute seed grant, as well as the NSF Grants Nos. DMR-0844115, DMR-0820579, and DMR-0847782. We also acknowledge discussions with N. Clark, J. Evans, Q. Liu, H. Mireles, K. Park, L. Radzihovsky, and R. Trivedi.

[1] H. Stark, Phys. Rep. **351**, 387 (2001).
[2] P. Poulin, H. Stark, T. C. Lubensky, and D. A. Weitz, Science **275**, 1770 (1997).
[3] P. Poulin and D. A. Weitz, Phys. Rev. E **57**, 626 (1998).
[4] I. I. Smalyukh, A. V. Kachynski, A. N. Kuzmin, and P. N. Prasad, Proc. Natl. Acad. U.S.A. **103**, 18048 (2006).
[5] Y. Gu and N. L. Abbot, Phys. Rev. Lett. **85**, 4719 (2000).
[6] P. S. Pershan and J. Prost, J. Appl. Phys. **46**, 2343 (1975).
[7] M. S. Turner and P. Sens, Phys. Rev. E **57**, 823 (1998).
[8] G. Liao, I. I. Smalyukh, J. R. Kelly, O. D. Lavrentovich, and A. Jakli, Phys. Rev. E **72**, 031704 (2005).
[9] C. D. Santangelo and R. D. Kamien, Phys. Rev. Lett. **91**, 045506 (2003).
[10] C. Bohley and R. Stannarius, Eur. Phys. J. E **23**, 25 (2007).
[11] P. Sens and M. S. Turner, J. Phys. (France) **7**, 1855 (1997).
[12] R. Pratibha, K. Park, I. I. Smalyukh, and W. Park, Opt. Express **17**, 19459 (2009).
[13] J. J. Storhoff, R. Elghanian, R. C. Mucic, C. A. Mirkin, and R. L. Letsinger, J. Chem. Soc. **120**, 1959 (1998).
[14] U. Kreibig and M. Völlmer, *Optical Properties of Metal Clusters* (Springer-Verlag, Berlin, 1995).
[15] C. F. Bohren and D. R. Huffman, *Absorption and Scattering of Light by Small Particles* (Wiley-Interscience, New York, 1983).
[16] V. Yannopapas and A. Moroz, J. Phys.: Condens. Matter **17**, 3717 (2005).
[17] J. B. Fournier, I. Dozov, and G. Durand, Phys. Rev. A **41**, 2252 (1990).
[18] V. Designolle, S. Herminghaus, T. Pfohl, and C. Bahr, Langmuir **22**, 363 (2006).
[19] P. G. de Gennes and J. Prost, *The Physics of Liquid Crystals* (Clarendon, Oxford, 1995).
[20] I. I. Smalyukh and O. D. Lavrentovich, Phys. Rev. Lett. **90**, 085503 (2003).
[21] S. Kubo, A. Diaz, Y. Tang, T. S. Mayer, I. C. Khoo, and T. E. Mallouk, Nano Lett. **7**, 3418 (2007).
[22] S. Biggs and P. Mulvaney, J. Chem. Phys. **100**, 8501 (1994).
[23] C. P. Lapointe, T. G. Mason, and I. I. Smalyukh, Science **326**, 1083 (2009).
[24] V. J. Anderson and H. N. Lekkerkerker, Nature (London) **416**, 811 (2002).
[25] I. I. Smalyukh, Y. Lansac, N. Clark, and R. Trivedi, Nature Mater. **9**, 139 (2010).
[26] M. Kleman and O. D. Lavrentovich, Liq. Cryst. **36**, 1085 (2009).